Journal of Colloid and Interface Science 380 (2012) 121–127

Contents lists available at SciVerse ScienceDirect

Journal of Colloid and Interface Science

www.elsevier.com/locate/jcis

Enhancement of photocatalytic activity of nano-scale TiO_2 particles co-doped by rare earth elements and heteropolyacids

Huixian Shi [a,b], Tianyong Zhang [b], Taicheng An [a], Bin Li [b,*], Xiao Wang [b]

[a] State Key Laboratory of Organic Geochemistry, Guangzhou Institute of Geochemistry, Chinese Academy of Sciences, Guangzhou 510640, China
[b] School of Chemical Engineering and Technology, Tianjin University, Tianjin 300072, China

ARTICLE INFO

Article history:
Received 11 February 2012
Accepted 22 April 2012
Available online 4 May 2012

Keywords:
TiO_2
Rare earth ion
Heteropolyacid
Co-doping
Photocatalytic activity

ABSTRACT

Nano-scale TiO_2 photocatalysts co-doped by rare earth ions (La^{3+}, Ce^{3+}) and heteropolyacids were designed and prepared by sol–gel method to probe synergistic effect on photocatalytic elimination of organic compounds, and their physicochemical properties were characterized by X-ray diffraction (XRD), specific surface area and porosity (BET and BJH), high resolution transmission electron microscopy (HRTEM), UV–vis diffuse reflectance spectroscopy (UV–vis DRS), and X-ray photoelectron spectroscopy (XPS) as well as Raman spectroscopy. The photocatalytic activity of prepared catalysts was evaluated by the degradation of methylene blue (MB) in water under UV-light irradiation. The results showed that the co-doping of the rare earth ions and heteropolyacids can significantly improve the photocatalytic activity of prepared composite photocatalysts due to the efficient inhibition of the recombination of photogenerated electron–hole pairs. The enhancement mechanism of co-doping of the rare earth ions and heteropolyacids on TiO_2 is also discussed.

1. Introduction

Photocatalytic oxidation techniques have attracted much attention to their potential application in water treatment, air purification, and sunlight utilization. Among numerous semiconductor materials, TiO_2 has been regarded as one of the most promising photocatalysts for the degradation of organic pollutants, because of its physical and chemical stability, low cost, no toxicity, and unique electronic and optical properties [1–4]. However, the utilization of pure TiO_2 is significantly constrained because of its wide band gap, low efficiency of sunlight utilization, low quantum efficiency, and high recombination rate of electrons-holes. Therefore, it is of great interest to improve the photocatalytic activity of TiO_2 in order to enlarge the practical applications of TiO_2-based photocatalysts [5,6].

Rare earth ions are well known for their ability to form complexes with various Lewis bases in the interaction of these functional groups with the *f*-orbital [7–9]. Thus, the incorporation of the rare earth ions into TiO_2 crystalline matrices could provide a potential means to inhibit the combination of photohole and photoelectron pairs and to enlarge the light adsorption of the semiconductor, and therefore to enhance the visible light photocatalytic activity, such as Eu-TiO_2 nanocrystalline [10], Ln_2O_3/TiO_2 (Ln = Eu, Pr, or Yb) [11], La-TiO_2, Pr-TiO_2, Nd-TiO_2 [12], N-Ce/TiO_2 [13]. The results indicated that the photocatalytic activity of TiO_2 could be significantly enhanced by doping with the rare earth ions because the doped rare earth ions can form complexes with various organic molecules by *f*-orbital.

On the other hand, heteropolyacids are a large variety of oxygen-bridged metal clusters which is well known for their rich photocatalytic action. Electrons are promoted from an orbital of oxygen to that of metal atom when UV-light was illuminated [14,15]. So heteropolyacids have been frequently used as photocatalysts in the oxidation or reduction of organic or inorganic compounds in water. Ozer has reported the use of heteropolyacids such as $PW_{12}O_{40}^{3-}$, $SiW_{12}O_{40}^{4-}$, and $W_{10}O_{32}^{4-}$ could facilitate the transfer of photogenerated electrons of TiO_2 conduction band to dioxygen as a means of increasing the efficiency of the photodegradation of 1, 2-dichlorobenzene [16], and another report also observed that the doping heteropolyacids into TiO_2 can increase eightfold in the apparent degradation rate of 1,2-dichlorobenzene compared to TiO_2 alone [17].

Thus, in the present work, in order to combine the above properties of the rare earth ions and heteropolyacids, the rare earth elements and heteropolyacids were both employed to co-doped TiO_2 via sol–gel method to obtain a cost-effective photocatalyst. To the best of our knowledge, this is the first report to fabricate a co-doped nano-scale TiO_2 photocatalyst both with the rare earth ions (La^{3+}, Ce^{3+}) and heteropolyacids ($H_3PW_{12}O_{40}$, $H_3PMo_{12}O_{40}$,). This work will optimize the preparation affecting factors and highlight the development of synergistic effect for the co-doped

* Corresponding author. Fax: +86 022 27406610.
E-mail address: libin@tju.edu.cn (B. Li).

0021-9797/$ - see front matter © 2012 Elsevier Inc. All rights reserved.
http://dx.doi.org/10.1016/j.jcis.2012.04.069

photocatalysts, Ce-$H_3PMo_{12}O_{40}/TiO_2$ and La-$H_3PW_{12}O_{40}/TiO_2$, which were further evaluated by the photocatalytic degradation of methylene blue (MB) under UV-light irradiation.

2. Experimental

2.1. Material

Tetrabutyl titanate $Ti(OC_4H_9)_4$, $La(NO_3)_3$, $Ce(NO_3)_3$, $H_3PMo_{12}O_{40}$, $H_3PW_{12}O_{40}$, acetic acid, absolute ethanol, nitric acid were all analytical reagents and supplied by Kewei Chemical Reagents Company (China).

2.2. Preparation of photocatalyst

Ce-$H_3PMo_{12}O_{40}/TiO_2$ was prepared by sol–gel method with the following procedure: Solution A: 34 mL $Ti(OBu)_4$ was dissolved in 44 mL absolute ethanol with stirring for 20 min, and then 3 mL acetic acid as hydrolysis suppressant was added. Solution B: $Ce(NO_3)_3$ and $H_3PMo_{12}O_4$ in the required stoichiometry were first dissolved in 44 mL absolute ethanol and 7.2 mL deionized water was added subsequently. Then, solution B was dropped into solution A slowly within 30 min. After that the mixture was hydrolyzed at 25 °C for 30 min under heavily agitation and then the transparent sol was obtained. The gelation was finished by aging this sol for 24 h at room temperature, and the gel was dried at 60 °C, then ground to powder and calcinated at different temperatures for 3 h. La-$H_3PW_{12}O_{40}/TiO_2$, La-TiO_2, Ce-TiO_2, $H_3PW_{12}O_{40}/TiO_2$, $H_3PMo_{12}O_{40}/TiO_2$, and pure TiO_2 were prepared with the same method as compared.

2.3. Characterization of photocatalyst

To determine the crystal phase composition of the prepared catalysts, X-ray diffraction (XRD) was carried out by using a PANAalytical X' pert Por X-ray diffractometer (Holland) with Cu Kα radiation. The diffract angles were recorded in the 2θ range 20–100° in steps of 0.017°. The specific surface area (BET method), the specific pore volume, and the average pore diameter (BJH method) of the catalysts were measured by N_2 adsorption–desorption isotherms by using Quantachrome NOVA-2000 sorption analyzer (USA), and the samples were analyzed at 77 K by nitrogen adsorption–desorption. Transmission electron microscopy (TEM) micrographs were obtained by using Philips Tecnai G2 F20 instrument (Holland). The UV–vis diffuse reflectance spectra (UV–vis DRS) were performed with a Lambda 900 UV–vis spectrophotometer (Perkin-Elmer). Raman spectra were recorded by Bruker RFS100/S Raman spectrometer (Germany). And the X-ray photoelectron spectroscopy (XPS) analyses of the samples were performed on a PHI-1600 ESCA spectrometer (USA) using 300 W Mg Kα radiation, and the binding energies were referenced to the C1s line at 284.8 eV from adventitious carbon.

2.4. Photocatalytic degradation

The photocatalytic activity of the catalysts was evaluated by degradation of MB. The initial concentration of MB was 40 mg L^{-1}. The photocatalytic reactor consists of a 160 mL Pyrex glass bottle with a jacket outside and a 125 W high pressure Hg lamp was used as light source in parallel to the reactor. In all experiments, the reaction temperature was kept at 25 ± 1 °C by a continuous circulation of water in the jacket around the reactor. Reaction suspensions were prepared by adding different amount of the photocatalyst powders into 50 mL MB aqueous solution under vigorous stirring. Prior to irradiation, all the reaction suspensions were stirred in dark for 20 min to establish an adsorption–desorption equilibrium. The samples were collected at regular irradiation intervals, and the concentration changes of MB solution were measured using a UV–vis spectrometer at 665 nm (λ_{max}). The activity of catalyst is evaluated by the degradation rate (D) of the samples. The equation of the degradation rate is followed:

$$D = \frac{A_0 - A_t}{A_0} \times 100\% \quad (1)$$

where D is the degradation rate, A_o is the initial absorbance of MB, and A_t is the absorbance of MB after "t" minutes.

3. Results and discussion

3.1. Characterization of the catalysts

The plot of N_2 adsorption–desorption isotherm and the Barrett–Joyner–Halenda (BJH) pore size distribution plot of the representative samples are given in Fig. 1a and b, respectively. It can be easily seen from the figure that the isotherm is of type IV curve with H1 hysteresis loop, which implies that the representative samples exhibit mesoporosity with a high degree of pore size uniformity with the average pore size approximately 5.5 nm and 3.5 nm, respectively [18]. The nitrogen adsorption–desorption isothermal curves show well-defined adsorption steps. At low relative pressure ($p/p_0 < 0.4$), the isotherms exhibit high adsorption, which indicated the powders are mesoporous particles. At a middle relative pressure ($p/p_0 = 0.4–0.8$), the curves exhibit a H1 hysteresis loop, which can further confirm the powders mesoporous photocatalysts. The specific surface area of the Ce-$H_3PMo_{12}O_{40}/TiO_2$ and La-$H_3PW_{12}O_{40}/TiO_2$ calcinated at 600 °C are 72 and 74 $m^2\,g^{-1}$,

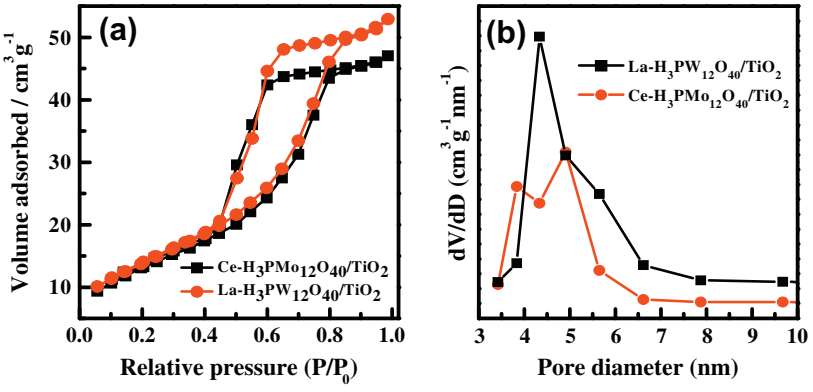

Fig. 1. Nitrogen adsorption–desorption isothermal (a) and pore size distribution plots (b) of Ce-$H_3PMo_{12}O_{40}/TiO_2$ and La-$H_3PW_{12}O_{40}/TiO_2$.

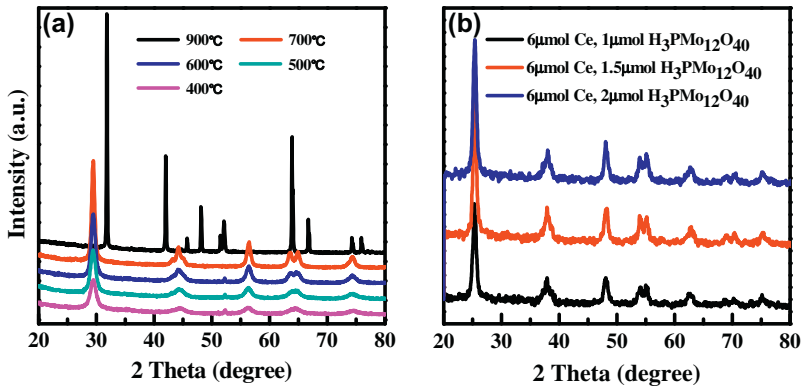

Fig. 2. XRD patterns of Ce-$H_3PMo_{12}O_{40}/TiO_2$ at different calcinated temperatures (a) and with different dopant amount (b).

respectively, which is much larger than that of pure TiO_2 ($30\ m^2\ g^{-1}$). Higher specific surface areas can improve the adsorption ability of photocatalysts, because the photocatalytic activity strongly depends on the better adsorption of organic substrate and the interfacial charge transfer can also be improved [19]. Huang et al. [20] have found that the high specific surface area of prepared photocatalysts improve from $30\ m^2\ g^{-1}$ to $150\ m^2\ g^{-1}$ with the increasing of the amount of $H_3PW_{12}O_{40}$. It is because mononuclear Ti—OH can form larger multinuclear ions without the addition of $H_3PW_{12}O_{40}$ in the system, but the condensate effect of prepared photocatalysts can be inhibited between Ti and OH with the addition of $H_3PW_{12}O_{40}$ in the system. Thus, the specific surface area is increased when the heteropolyacids were doped into TiO_2.

The wide-angle XRD patterns of obtained samples are presented in Fig. 2 and Fig. S1. The peaks at 25.4°, 37.8°, and 48.1° elucidate the diffractions of the (101), (004), and (200) anatase-type TiO_2, which can be indexed as the anatase phase of TiO_2 (PDF21-1272), whereas the XRD peaks at 27.4° (110) and 54.5° belong to rutile form. As shown in Fig. 2b and Fig. S1b, the XRD patterns of Ce-$H_3PMo_{12}O_{40}/TiO_2$ and La-$H_3PW_{12}O_{40}/TiO_2$ calcinated at 600 °C are all the anatase phase absolutely, and almost no rutile phase is observed. The ones doping with heteropolyacids and the rare earth ions can prevent the formation of rutile phase. No peaks related to the separated heteropolyacids and the rare earth ions were observed, because the crystalline dimension of heteropolyacids and rare earth ions dispersing onto the TiO_2 surface is lower than the detection limit of the instrument. The diffraction peaks of the samples calcinated from 400 °C to 900 °C were also recorded. As shown in Fig. 2a and Fig. S1a, the peaks intensity of anatase increase with the increase of calcination temperature from 400 °C to 900 °C, and the width of (101) plane becomes narrow, and the phase transformation from anatase to rutile phase occurred at 900 °C. Thus, the dopant is expected to play a significant role in the selective crystallization of anatase phase. Table S1 shows the mean crystal sizes of the samples at different calcinated temperatures calculated with Scherrer formula [21]. It can be seen that the average crystallite size of the anatase phase TiO_2 increased with increasing calcination temperature. It was concluded that the rare earth ions and heteropolyacids doping could hinder crystal transformation and decrease crystallite size, generally, which the smaller crystalline size could lead to larger surface area.

Raman spectra of the obtained photocatalysts were presented in Fig. 3, and the characteristic peaks at 154.4 (E_g), 403.2 (B_{1g}), 523.4 (B_{1g}), and 645.7 cm^{-1} (E_g) as shown in figure were originated from the anatase phase of TiO_2 [22]. As for the Ce-$H_3PMo_{12}O_{40}/TiO_2$ and La-$H_3PW_{12}O_{40}/TiO_2$ composite photocatalysts, above mentioned four peaks corresponding to the anatase phase TiO_2 were further confirmed by the anatase structure of prepared TiO_2 as a control in this paper. However, the E_g of TiO_2 Raman mode at 154.4 cm^{-1} shifted to lower wave numbers, that is, from 154.4 cm^{-1} at TiO_2 to 150.8 cm^{-1} for Ce-$H_3PMo_{12}O_{40}/TiO_2$ and 145.9 cm^{-1} for La-$H_3PW_{12}O_{40}/TiO_2$, respectively. From Raman spectra, we also find the Keggin unit-relating peaks. Thus, the $H_3PW_{12}O_{40}$ relating Raman peaks were assigned as follows: 1001.6 cm^{-1} (strong) is corresponding to symmetric P-O bond stretching vibrations of the PO_4 site [23] and 977 cm^{-1} (weak) is corresponding to W=O bond stretching vibrations, and then 926 cm^{-1} (weak) is also corresponding to W—O—W bond stretching vibrations. In the Raman spectrogram of La-$H_3PW_{12}O_{40}/TiO_2$, the peaks corresponding to W=O and P—O bonds vibrations were broadened; therefore, only one wide peak in the range of 959.8–

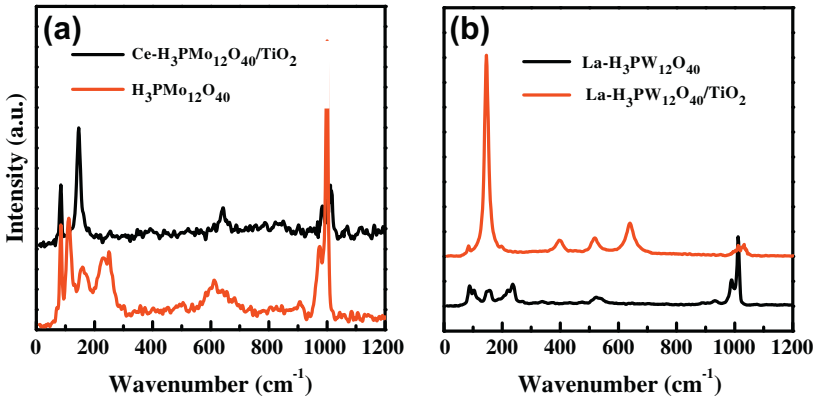

Fig. 3. Raman spectra of the samples.

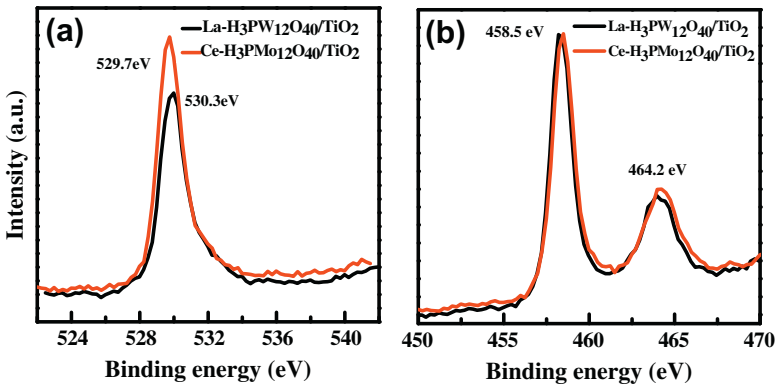

Fig. 4. O1s (a) and Ti 2p (b) high resolution XPS of La-$H_3PW_{12}O_{40}/TiO_2$ and Ce-$H_3PMo_{12}O_{40}/TiO_2$.

1058.1 cm^{-1} was obtained. At the same time, the peak intensity corresponding to W—O—W bond vibrations become much weaker, and similar results were found in $H_3PMo_{12}O_{40}$ and Ce-$H_3PMo_{12}O_{40}/TiO_2$ composite photocatalysts. The above changes of Raman shifts and the decreases of the peak intensities are due to strong interactions between the Keggin unit and anatase phase TiO_2 network, resulted in the decrease of the symmetry of either TiO_2 or heteropolyacids molecules.

To evaluate the surface state of composite photocatalysts, the prepared samples were characterized by XPS. The high resolution XPS of O1s and Ti2p in La-$H_3PW_{12}O_{40}/TiO_2$ and Ce-$H_3PMo_{12}O_{40}/TiO_2$ is shown in Fig. 4. The binding energy of O1s is about 529.7 and 530.3 eV, respectively, which has a bit of deviation compared with pure TiO_2 (529.4 eV). This indicated that the doping ions affect the binding energy of Ti—O bond. The perhaps reason is considered a vacant oxygen attributed to the substitution of the doping ions of Ti^{4+}. The Ti 2p levels of all samples show two peaks at approximately 464.2 and 458.5 eV, which are assigned as $Ti2p^{1/2}$ and $Ti2p^{3/2}$ of TiO_2. It indicates that the Ti element mainly exists as the chemical state of Ti^{4+} [4]. The high resolution of Ce3d and Mo3d in Ce-$H_3PMo_{12}O_{40}/TiO_2$ is also presented in Fig. 5, and the binding energy of $Ce3d^{5/2}$ at about 883.5 eV, which is higher than that of pure Ce_2O_3 due to the Ce^{3+} going into the crystal lattice of TiO_2 to form Ti—O—Ce bond. The binding energy of Mo3d is in accordance with Mo^{6+}, so the Mo element is of the form of Mo^{6+} on the surface of catalyst. The high resolution XPS of La3d (a) and W4f (b) in La-$H_3PW_{12}O_{40}/TiO_2$ is displayed in Fig. S2. The La atoms existed in the form of La^{3+} valences in the sample, and the main peaks at 834.9 eV are well in accordance with the standard XPS peaks of La^{3+}. The resulting W 4f XPS spectra are also shown in Fig. S2b and are characteristic of high oxidation state tungstate environments. These divided spectra reveal a broad, doublet centered peak around 35.7 ($4f^{5/2}$ component) and 37.9 eV ($4f^{7/2}$ component), which is consistent with that in the pure parent $H_3PW_{12}O_{40}$ heteropoly acid [24,25]. Meanwhile, from the XPS data we can estimate that the relative surface atomic percentage of O, Ti, Mo, and Ce in Ce-$H_3PMo_{12}O_{40}/TiO_2$ is 43.6%, 15.1%, 0.8%, and 0.7%, respectively, and the percentage of O, Ti, W, and La is 41.7%, 12.5%, 0.7%, and 0.5%, respectively, in La-$H_3PW_{12}O_{40}/TiO_2$.

To further investigate the optical absorption properties of catalysts, the UV–vis DRS of prepared Ce-$H_3PMo_{12}O_{40}/TiO_2$ and La-$H_3PW_{12}O_{40}/TiO_2$ were measured in the range of 200–800 nm and the results are shown in Fig. 6. The strong adsorption at 200–300 nm is the characteristic of TiO_2, and the catalysts with doped heteropolyacids and the rare earth ions can clearly shift the adsorption band toward the visible range. The absorbance variation increases with the increase of doping heteropolyacids and the rare earth ions. Red shift of this type can be attributed to the charge-transfer transition between *f* electrons of rare earth ions and TiO_2 conduction or valence band. The synergistic effect may exist between rare earth ions, heteropolyacids, and the anatase TiO_2 because both the rare earth ions and heteropolyacids can affect electron transformation in TiO_2 photocatalytic systems, acted as the electron shuttles in light illuminating TiO_2 [26]. In addition, it can be noted that the optical absorption intensity in the UV region is also enhanced, which is consistent with the conclusion of the doping of rare earth ions into TiO_2 by Yan et al. [27]. The band gap energy of prepared catalysts estimated from Fig. S5, it can be found that the band gap of the prepared catalyst was decreased as the amount of rare earth ion and heteropolyacids increased, which can extend to the visible light region.

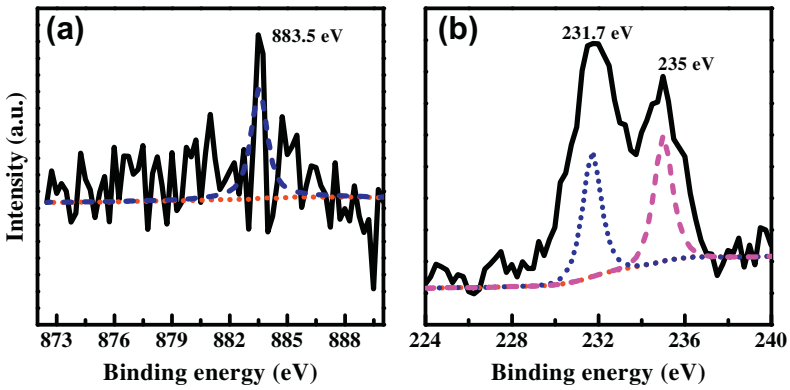

Fig. 5. Ce3d (a) and Mo3d (b) high resolution XPS of Ce-$H_3PMo_{12}O_{40}/TiO_2$.

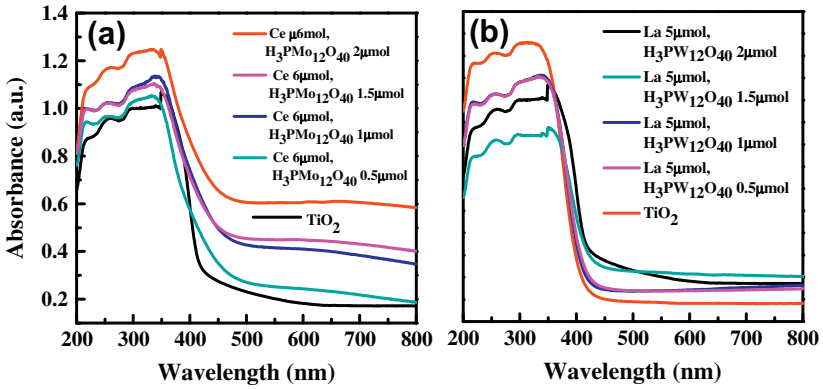

Fig. 6. UV–vis DRS spectra of the samples, (a) pure TiO_2 and Ce-$H_3PMo_{12}O_{40}/TiO_2$ with different dopant amount; (b) pure TiO_2 and La-$H_3PW_{12}O_{40}/TiO_2$ with different dopant amount.

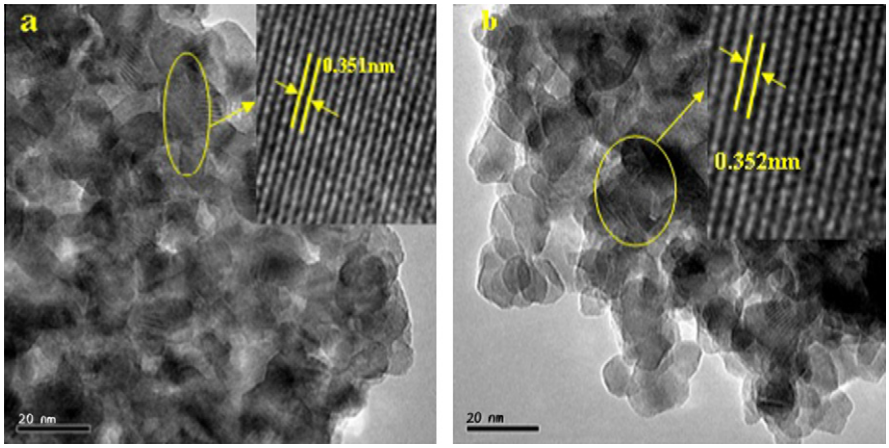

Fig. 7. HRTEM of Ce-$H_3PMo_{12}O_{40}/TiO_2$ (a) and La-$H_3PW_{12}O_{40}/TiO_2$ (b).

Fig. 7 also shows the HRTEM micrographs of the prepared photocatalysts. As can be seen, the samples have a relative uniform particle diameter distribution in the range of 10–30 nm. Furthermore, the nanoparticles with mesoporous characteristic can be observed more clearly from the HRTEM. The HRTEM images show the surface micrographs of prepared photocatalysts, where the set of fringes corresponds to the (101) lattice planes of anatase phase TiO_2. Thus, it proved that anatase phase has well formed in the mesoporous composite photocatalysts. It is difficult to identify the heteropolyacids particles on the TiO_2 surface, so the EDX of the prepared catalysts were measured and the results were shown in Fig. S3 and S4 in supporting information. Seen from the Fig. S3 and S4 that there were Ce, Mo, Ti, and O elements on the surface of the Ce-$H_3PMo_{12}O_{40}/TiO_2$, as well as La, W, Ti, and O elements on the surface of the La-$H_3PW_{12}O_{40}/TiO_2$. So we could confirm that the heteropolyacids and rare earth ions presented on the TiO_2 surface.

3.2. Photocatalytic activity of degradation of MB

The photocatalytic activity of prepared catalysts was determined by the degradation of MB in water. As shown in Fig. 8 that the photocatalytic adsorption capacities and the degradation efficiency of Ce-$H_3PMo_{12}O_{40}/TiO_2$ and La-$H_3PW_{12}O_{40}/TiO_2$ are higher than those of Ce-TiO_2, La-TiO_2, $H_3PMo_{12}O_{40}/TiO_2$, and $H_3PW_{12}O_{40}/TiO_2$, and an obviously synergistic effect was obtained when Ce-$H_3PMo_{12}O_{40}/TiO_2$ and La-$H_3PW_{12}O_{40}/TiO_2$ were used as photocatalysts. The degradation efficiency of 98% was obtained with photocatalyst containing 6 µmol Ce^{3+} and 2 µmol $H_3PMo_{12}O_{40}$ in Ce-$H_3PMo_{12}O_{40}/TiO_2$, while the highest degradation efficiency of 96% was obtained when the La-$H_3PW_{12}O_{40}/TiO_2$ containing 5 µmol La^{3+} and 1.5 µmol $H_3PW_{12}O_{40}$ in 1 mol TiO_2 was used as photocatalyst. As-prepared mesoporous Ce-$H_3PMo_{12}O_{40}/TiO_2$ and La-$H_3PW_{12}O_{40}/TiO_2$ catalysts all showed high BET surface areas, which resulted in an increase of photocatalytic activity by providing more contact

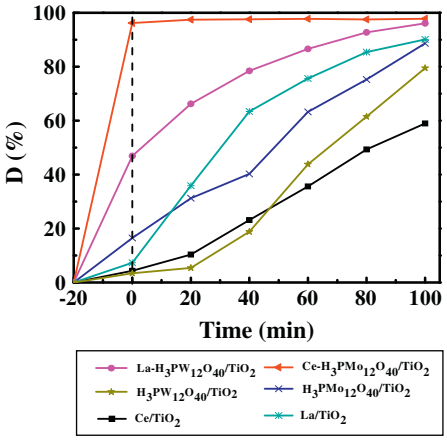

Fig. 8. Photocatalytic activity of prepared catalysts ($[MB]_o$ 40 mg L^{-1}, catalyst calcinated at 600 °C and dosage is 0.2 g/50 mL).

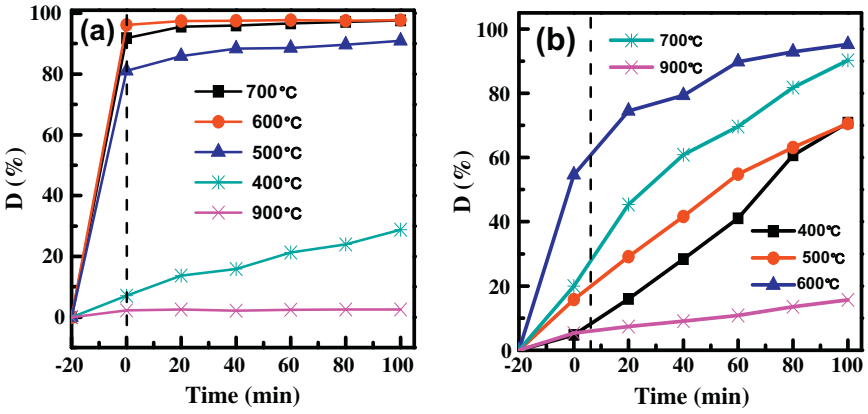

Fig. 9. Effect of calcination temperature of Ce-$H_3PMo_{12}O_{40}/TiO_2$ (a) and La-$H_3PW_{12}O_{40}/TiO_2$ (b).

areas between the catalyst and the substrate MB. The heteropolyacids doping can destroy the charge balance of catalysts surface, and a lot of OH^- was adsorbed into the catalysts surface for keeping charge balance. Meanwhile, the OH^- can accept the photogenerated hole, so it can inhibit the recombination of electron–hole pair and improve the photoactivity effectively. On the other hand, the holes based on $H_3PW_{12}O_{40}$ and $H_3PMo_{12}O_{40}$ have strong oxidation power, and consequently, it is reduced to PW_12^- and PMo_{12}, which absorbs UV light and obtains stronger reduction power.

To study the effect of catalyst structure on photodegradation, the calcinated temperatures to prepare photocatalysts were also investigated. It is shown in Fig. 9 that the degradation efficiency was declined with the increasing the calcinated temperature, and the highest degradation efficiency over 98% was achieved with the photocatalyst calcinated at 600 °C, because the well crystalloid anatase structure TiO_2 has a better photocatalytic activity. But the prepared photocatalysts became aggregation and the rutile phase was formed when the calcinated temperature was increased, so the photocatalytic activity of these prepared photocatalysts declines slowly. It is interesting that the adsorption capacity of Ce-$H_3PMo_{12}O_{40}/TiO_2$ is stronger than that of La-$H_3PW_{12}O_{40}/TiO_2$ when both are calcined at 500 °C, 600 °C, 700 °C, because the valent state of Ce can transform from Ce^{3+} into Ce^{4+}. Thus, the amount of photogenerated electron must be changed during the transform [28], which is beneficial for the adsorption of the substrate.

3.3. Photocatalytic reaction mechanism

According to the mechanism of TiO_2 photocatalysis, photogenerated electron–hole pairs are formed when photocatalyst is irradiated by super band gap light, and the electron and hole will overcome their mutual electrostatic attraction and become spatially separated, and then diffuse to the surface, where the electron will be captured by O_2 and the hole will be transferred by adsorbed hydroxide to form ·OH radicals. However, there is a high chance of the recombination of the electrons and holes which is the important source of inefficiency in TiO_2 photocatalytic systems. But rare earth ions and heteropolyacids co-doping lead to a new electronic state in the middle of the TiO_2 band gap, the introduction of structural defects into the TiO_2 crystal lattice leads to the change of band gap energy [8]. The schematic diagram of the photocatalytic mechanism is shown in Fig. 10. The electrons, which are excited from the valence band of prepared composite photocatalysts after absorbing UV-light photons, were captured by heteropolyacids in the doped catalysts at first, and the heteropolyacids can be acted as an electron scavenger to retard the fast charge recombination with electron hole (h^+) in reaction system, consequently, to enhance the photocatalytic redox processes [29]. In addition, the heteropolyacids ions, which are generated from electron reduction reaction by e^-_{CB} in the surface of catalysts can also consequently synergistically catalyze the substrate molecules. Furthermore, co-

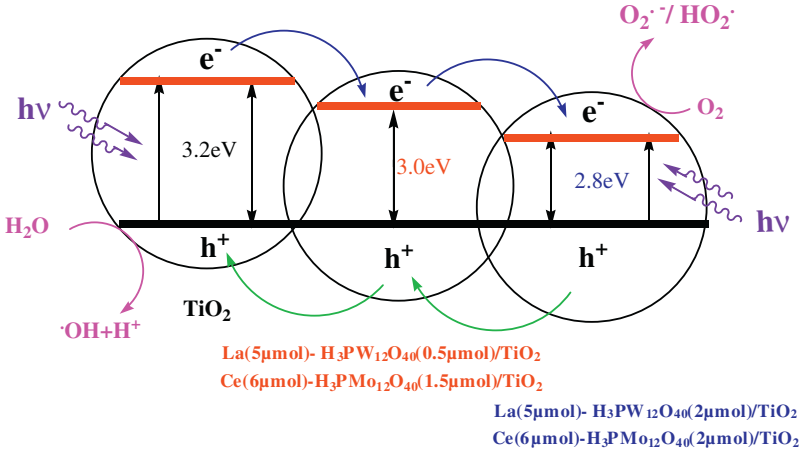

Fig. 10. Photocatalysis mechanism schematic diagram of La-$H_3PW_{12}O_{40}/TiO_2$ and Ce-$H_3PMo_{12}O_{40}/TiO_2$ reaction systems.

doping with the rare earth ions and heteropolyacids can decrease the band gap of TiO_2, which can enhance the efficiency of sunlight utilization and quantum efficiency.

4. Conclusions

The rare earth elements and heteropolyacids co-doped composite photocatalysts, Ce-$H_3PMo_{12}O_{40}/TiO_2$ and La-$H_3PW_{12}O_{40}/TiO_2$, were prepared by sol–gel method. The catalysts have much larger specific surface area as compared with pure TiO_2, which can significantly enhance the substrate adsorption. Co-doped with the rare earth ions and heteropolyacids into TiO_2 not only suppressed the crystal growth of TiO_2 but also prevented phase transition of anatase to rutile. The prepared photocatalysts have higher photocatalytic activity for the degradation of MB as compared to pure TiO_2 which is due to the synergistic effect existed between the rare earth ions and heteropolyacids as well as the anatase TiO_2, which can enlarge the light adsorption and inhibit the recombination of photogeneration electron–hole pairs. Hence, we emphasize that to improve the synergistic effect of multicomponent is a desirable way to overcome the limitation of the low quantum efficiency and to avoid high recombination rate of electrons-holes of the photocatalyst.

Acknowledgments

This is contribution No. IS−1501 from GIGCAS. This work was supported by National Natural Science Foundation of China (Grant No. 21103121) and Research Fund for the Doctoral Program of Higher Education of China (Grant No. 20110032120011) to T.Y. Zhang and B. Li, and the Science and Technology Project of Guangdong Province, China (2011A030700003 and 2010B090300017, 2009B091300023 and 2009A030902003) to T. C. An.

Appendix A. Supplementary material

Supplementary data associated with this article can be found, in the online version, at http://dx.doi.org/10.1016/j.jcis.2012.04.069.

Reference

[1] S. Kitano, K. Hashimoto, H. Kominami, Appl. Catal. B 101 (2011) 206.
[2] T. An, W. Zhang, X. Xiao, G. Sheng, J. Fu, X. Zhu, J. Photochem. Photobio. A: Chem. 161 (2004) 233.
[3] H. Yang, G.Y. Li, T.C. An, Y.P. Gao, J.M. Fu, Catal. Today 153 (2010) 200.
[4] Y. Zhang, Z.R. Tang, X. Fu, Y.J. Xu, Appl. Catal. B 106 (2011) 445.
[5] D. Masih, H. Yoshitake, Y. Izumi, Appl. Catal. A: Gen. 325 (2007) 276.
[6] T. An, J. Liu, G. Li, S. Zhang, H. Zhao, X. Zeng, G. Sheng, J. Fu, Appl. Catal. A: Gen. 350 (2008) 237.
[7] A.W. Xu, Y. Gao, H.Q. Liu, J. Catal. 207 (2002) 151.
[8] Y. Xie, C. Yuan, Appl. Catal. B: Environ. 46 (2003) 251.
[9] S. Yuan, Q. Sheng, J. Zhang, F. Chen, M. Anpo, Q. Zhang, Micropor. Mesopor. Mater. 79 (2005) 93.
[10] Y. Zhang, H. Zhang, Y. Xu, Y. Wang, J. Mater. Chem. 13 (2003) 2261.
[11] K.T. Ranjit, I. Willner, S.H. Bossmann, A.M. Braun, Environ. Sci. Technol. 35 (2001) 1544.
[12] K.M. Parida, N. Sahu, J. Mol. Catal. A: Chem. 287 (2008) 151.
[13] X.Z. Shen, Z.C. Liu, S.M. Xie, J. Guo, J. Hazard. Mater. 162 (2009) 1193.
[14] G. Marcì, E. García-López, L. Palmisano, D. Carriazo, C. Martín, V. Rives, Appl. Catal. B: Environ. 90 (2009) 497.
[15] Y. Yang, Y. Guo, C. Hu, E. Wang, Appl. Catal. A: Gen. 252 (2003) 305.
[16] R.R. Ozer, J.L. Ferry, Environ. Sci. Technol. 35 (2001) 3242.
[17] C. Chen, P. Lei, H. Ji, W. Ma, J. Zhao, H. Hidaka, N. Serpone, Environ. Sci. Technol. 38 (2003) 329.
[18] J. Liu, T.C. An, G.Y. Li, N.Z. Bao, G.Y. Sheng, J.M. Fu, Micropor. Mesopor. Mater. 124 (2009) 197.
[19] L. Pan, J.J. Zou, X.W. Zhang, L. Wang, J. Am. Chem. Soc. 133 (2011) 10000.
[20] D. Huang, Y.J. Wang, L.M. Yang, G.S. Luo, Micropor. Mesopor. Mater. 96 (2006) 301.
[21] M. Zhang, T. An, X. Hu, C. Wang, G. Sheng, J. Fu, Appl. Catal. A: Gen. 260 (2004) 215.
[22] L. Miao, S. Tanemura, S. Toh, K. Kaneko, M. Tanemura, J. Cryst. Growth 264 (2004) 246.
[23] N. Imanaka, T. Masui, H. Hirai, Chem. Mater. 15 (2003) 2289.
[24] A.D. Newman, A.F. Lee, K. Wilson, N.A. Young, Catal. Lett. 102 (2005) 45.
[25] P.A. Jalil, M. Faiz, N. Tabet, N.M. Hamdan, Z. Hussain, J. Catal. 217 (2003) 292.
[26] H. Park, W. Choi, J. Phys. Chem. B 107 (2003) 3885.
[27] Q.Z. Yan, X.T. Su, Z.Y. Huang, C.C. Ge, J. Eur. Ceram. Soc. 26 (2006) 915.
[28] X.-Z. Shen, Z.-C. Liu, S.-M. Xie, J. Guo, J. Hazard. Mater. 162 (2009) 1193.
[29] T. Tachikawa, M. Fujitsuka, T. Majima, J. Phys. Chem. C 111 (2007) 5259.